Materials Science

http://www.aimspress.com/journal/Materials

Research article

Fe-TiO$_2$/zeolite H-A photocatalyst for degradation of waste dye (methylene blue) under UV irradiation

Ririn Cahyanti, Sumari Sumari*, Fauziatul Fajaroh, Muhammad Roy Asrori and Yana Fajar Prakasa

Department of Chemistry, Faculty of Mathematics and Natural Sciences Universitas Negeri Malang, Jl. Semarang No. 5, Malang, 65145, Indonesia

* Correspondence: Email: sumari.fmipa@um.ac.id; Tel: +62 81333911567.

Abstract: Industrial wastewater contains non-biodegradable dyes that are highly toxic to humans and aquatic life. As solution from photocatalytic degradation, TiO$_2$ is one of the effective photocatalysts for wastewater degradation, but it has low adsorption power. To overcome this deficiency, this study synthesized a new photocatalyst by Fe-TiO$_2$/zeolite H-A. The photocatalyst was successfully synthesized by the impregnation method and was systematically characterized by XRD, XRF, SEM, FT-IR and UV-Vis DRS. XRD diffractogram at 2θ = 25.3 ° showed anatase phase of the photocatalyst. SEM results showed a rough and soft surface with a size of 491.49 nm. FT-IR analysis obtained the zeolite-A characteristic band, vibration of Ti-O-Ti groups and the vibration of the Fe-O group. The bandwidth of the band gap was 3.16 eV. The photocatalytic efficiency of methylene blue degradation reached 89.58% yield with optimum conditions: irradiation time of 50 min, pH 9 and concentration of methylene blue about 20 mg/L. Fe-TiO$_2$/zeolite H-A as a new photocatalyst can be an alternative photocatalyst to purify methylene blue.

Keywords: dye degradation; photocatalyst; TiO$_2$; zeolite A; ferrous material

1. Introduction

Textile dye come from the dyeing process, in which 10–15% of the used dyes cannot be recycled that still contain non-degradable dyes [1,2]. This is because the structure of the textile dye has one or more azo groups (R–N=N–R′) and an aromatic ring which are mostly replaced by a

sulfonate group and an aromatic structure [3]. Therefore, waste dye must be separated before it is discharged into rivers.

Several methods of removing waste dye, known as Advanced Oxidation Processes (AOPs), have been developed previously, including physical, biological and chemical process such as ultra-filtration, reverse osmosis, adsorption, coagulation, flocculation, ozonation, membrane filtration, biological treatment, chemical oxidation, electrochemistry and ion exchange [4,5]. However, the technique has several disadvantages, such as high cost, high chemical dosage and incompetent separation results, because it produces secondary wastes (by-products) such as sulfonates, phenols and many aromatic compounds which are more toxic than the initial wastewater contaminants [6]. The removal technique by photocatalytic degradation is reported as one of the appropriate and efficient techniques because the separation does not produce secondary contaminants [7,8]. The photocatalytic degradation process occurs when electron-hole pairs (e^- and h^+) interact with industrial wastes to produce highly reactive hydroxyl radicals (OH•), which are capable of oxidizing various contaminants (organic compounds) into simpler molecules such as CO_2, H_2O and low levels of acidic minerals [6,9,10].

Titanium (IV) oxide (TiO_2) is one of the important semiconductor compounds for photocatalysts because of its high photocatalytic activity, low toxicity, good electrochemical properties, excellent chemical stability, high redox potential, non-toxicity, inexpensiveness, erosion-resistance, abundance in nature, excellent stability over a wide pH range and environmental friendliness [11–14]. One TiO_2 phase is the anatase phase, which has bandgap energies of 3.2 eV [15,16]. Fe^{3+} ion sources are abundant in nature, cheap and easy to modify [17]. Fe^{3+} can reduce the recombination rate of electron and hole pairs [18] and establish energy levels inside the forbidden band gap [19]. Fe^{3+} cations have a smaller ionic radius of 0.55 Å compared to Ti^{4+} cations (0.61 Å) and are expected to be able to partially replace Ti^{4+} cations in the TiO_2 lattice structure. In the previous study, 1.75 wt% $Fe-TiO_2$ nanoparticles (anatase phase) were used for photocatalytic degradation of Methylene Blue at about 76% with conditions of 0.03 g/L catalyst dosage, 30 mg/L Methylene Blue (50 mL), UV lamp and 2 h reaction [20]. For increasing the degradation efficiency, zeolite can be an option, because it can delocalize excited electrons of TiO_2 and minimize e^-/h^+ recombination [21,22].

Zeolite Linde Type A (Zeolite LTA or zeolite A) is a synthetic zeolite with a very small pore diameter of 4 Å. Zeolite A is generally synthesized in the form of Na-zeolite with the formula $Na_{12}[(AlO_2)_{12}(SiO_2)_{12}] \cdot 27H_2O$ and has a 3D pore structure consisting of a sodalite cage connected through a hollow double ring 4 (D4R) of $[SiO_4]^{4-}$ and $[AlO_4]^{5-}$. 3D structure: D4R, sodalite cage and α-cage [23]. The pore diameter of zeolite A is 0.23–0.42 nm, and it has a Si/Al molar ratio of 1 or close to 1 [23]. The property advantages of zeolite A were low molar ratio, low cost and high thermal stability. Therefore, zeolite A has great potential for separation, catalyst, adsorbent and wastewater treatment applications [24].

The research carried out synthesis of a photocatalyst by adding 2 materials at once: Fe^{+3} ions are impregnated into TiO_2 (anatase phase), known as $Fe-TiO_2$, and it is then impregnated into Zeolite H-A. The purpose of this research is to investigate and study the photocatalyst TiO_2 with the modification of the addition of Fe metal and zeolite H-A (called $Fe-TiO_2$/Zeolite H-A), by confirmation of the results of XRD, XRF, SEM, FT-IR and UV-DRS. In addition, another objective is to study the resulting photocatalytic activity. The photocatalyst activity of $Fe-TiO_2$/zeolite H-A was studied by using it for the degradation of methylene blue dye as a model pollutant. The photocatalytic performance of the synthesized photocatalyst was investigated under UV. The

degradation was carried out with several parameters of contact time, pH and initial concentration of dye. In addition, until now, the development of photocatalysts with the addition of metal and a porous matrix (zeolite) as well as with TiO_2 is still rarely done.

2. Materials and methods

All reagents were used from analytical grade: Zeolite A (Merck), ammonium chloride (NH_4Cl 1 M), TiO_2 powder (Sigma Aldrich), $Fe(NO_3)_3 \cdot 9H_2O$ (Sigma Aldrich), ethanol (99%), demineralized water.

2.1. Preparation of zeolite A

Preparation of zeolite A was carried out using the ion exchange method. The process was assisted with an acid solution to obtain zeolite H-A. First, 5 g of zeolite Na-A was added, and then 50 mL of 1M NH_4Cl (1:10) was added with stirring using a shaker for 1 h at 150 rpm. After that, it was allowed to stand for 24 h. The mixture was filtered and neutralized with demineralized water to get a neutral pH. After that, the powder (residue) was dried in an oven at 115 ℃ for 2 h. The dried powder was calcined at 450 ℃ for 4 h. The calcined powder was zeolite H-A.

2.2. Synthesis of Fe-TiO₂/zeolite H-A

Synthesis of Fe-TiO_2/zeolite H-A photocatalyst was begun with the synthesis of Fe-TiO_2. The synthesis of Fe-TiO_2 was carried out with a modified method [25]. The synthesis method was the impregnation method. $Fe(NO_3)_3 \cdot 9H_2O$ powder was added to TiO_2 powder with 3% of TiO_2 weight in 100 mL of demineralized water. The solution was stirred with a magnetic stirrer for 1 hour and then heated at a temperature of 80–90 ℃. The residue was centrifuged and washed with demineralized water to pH 7. The obtained solid was then calcined at 400 ℃ for 2 h. Furthermore, the synthesis of Fe-TiO_2/zeolite H-A was carried out by a modified method [26]. 1.4 g of Fe-TiO_2 and 8 g of zeolite H-A were added into 10 mL of ethanol with stirring for 5 h. The mixture was filtered and neutralized. The residue was dried in an oven at 120 ℃ for 5 h. The solid was then calcined at 450 ℃ for 3 h.

2.3. Characterization for Fe-TiO₂/zeolite H-A

Crystal structure and phase were identified by Powder X-ray Diffraction (PXRD) (PANanalytical E'xpert Pro). The crystalline element content was analyzed by X-ray Fluorescence (XRF) (brand: PANalytical; type: Minipal 4). Surface morphology analysis with various magnifications was performed by Scanning Electron Microscopy (SEM) (FEI Inspect-S50). Functional group investigations were carried out by Fourier Transform Infra-Red (FT-IR) (Shimadzu IRPrestige 21). UV-Vis DRS (Analytik Jena Specord 200 plus) with a wavelength of 1100–200 nm was used to obtain band gap values, absorbance data. The obtained data was then processed using the Tauc plot equation with Origin software.

2.4. Photocatalytic degradation of Methylene Blue

The photocatalytic degradation process with UV irradiation was carried out in a cube-shaped box. All sides of the box covered in the dark (black light) box, and a 20-watt UV lamp was used. A stirrer was provided in the cube as a stirring device.

The degradation process was carried out as follows: 50 mg of Fe-TiO$_2$/zeolite H-A photocatalyst was put into a 50 mL Beaker glass. 10 mg/L of methylene blue was pipetted and diluted to 25 mL. Then, methylene blue was added to the photocatalyst. The mixture was stirred and irradiated with UV for 10–50 min with an interval of 10 min. After the irradiation process, the suspension was filtered to separate the supernatant and the precipitate. The supernatant obtained from each beaker was measured for absorbance with a UV-Vis spectrophotometer at a wavelength of 664 nm. The absorbance value obtained was then analyzed to get the linear regression equation, so the optimum time was obtained. The obtained data was then used in the formula for the percentage of degradation (Efficiency percentage) through the following equation.

$$Efficiency\ percentage = \frac{C_0 - C_t}{C_0} \times 100 \tag{1}$$

C_o and C_t are the initial concentration of methylene blue and the concentration after the degradation process, respectively. The same procedure was repeated for pH (3, 5, 7, 9) and concentration of methylene blue (10, 20, 30, 40, 50 mg/L).

3. Results and discussions

3.1. Activation of zeolite A

In Zeolite H-A form, the acidic site in the zeolite framework transformed into a soft acid site (zeolite H-A), so it is more easily substituted by Ti^{4+} ions [27]. On the other hand, zeolite pretreatment or zeolite activation is to reduce impurities that cover the external surface and pores of the zeolite [28]. The modification of zeolite A to zeolite H-A was carried out using a solution of ammonium chloride (NH$_4$Cl) through the ion exchange method. The ion exchange process occurs between metal cations alkali metals (Na$^+$, K$^+$) and alkaline earths (Ca$^+$, Ba^{2+}) with ammonium cations (NH^{4+}) from HH$_4$Cl, because metal cations have weak ion-dipole interactions with zeolites. The interactions support ion-exchange as shown in XRF results (Table 1) [29].

The XRD results are shown in Figure 1. Based on Figure 1, diffraction peaks of raw material appear at 2θ = 10.24°, 12.53°, 16.19°, 20.51°, 21.76°, 24.09°, 26.22°, 27.22°, 30.95°, 32.66°, 33.49° and 34.29°, which have the same crystal characteristics as zeolite A or zeolite Linde Type A (LTA) as the ICSD database No. 150097. This confirmed that the used raw material of zeolite was zeolite A. The XRD pattern of the zeolite H-A (Figure 1b) showed no peak shift and no significant diffractogram changes. This showed that the treatment of zeolite A to zeolite H-A did not change the crystal structure of the zeolite and the crystal phase compared to the initial zeolite. In addition, Figure 1 showed a fairly sharp diffraction peak, and this indicated the formation of zeolite H-A.

Based on the FT-IR results (Figure 1), the spectrum of zeolite LTA material appeared. The presence of the OH group of H$_2$O was indicated by the absorption band at 3365 cm^{-1} (bending vibration). The stretching vibration of the OH group of the silanol group (Si-OH) was shown in the

absorption band of 1648 cm^{-1}. The absorption bands of the O-T-O group (T = Si, Al) were shown at 677 cm^{-1} (symmetrical) and 1000 cm^{-1} (asymmetrical). The absorption at 552 cm^{-1} indicated the external vibration of the double ring (D4R or D6R), which is a characteristic of the zeolite LTA structure [30]. The absorption band at 475 cm^{-1} indicated a bending vibration of the T-O group (T = Si, Al), and the absorption band at 400–370 cm^{-1} indicated the open pores of the zeolite framework material [31]. Furthermore, the FT-IR spectrum of the zeolite H-A showed a slight shift in the absorption wavenumber and intensity, so it did not have much different results from the initial zeolite A. The absorption band at 1400–400 cm^{-1} appeared in the zeolite H-A spectrum; the absorption band is a typical absorption band of LTA zeolite (zeolite A) [32]. This shows that the preparation process of zeolite A to zeolite H-A was successful without damaging the structure of the zeolite.

Supporting data confirmed by looking at changes in the level of elemental composition in the zeolite using XRF characterization. The XRF results are shown in Table 1. The data was used to calculate the Si/Al zeolite ratio. It was known that the ratio of Si/Al zeolite from zeolite A to H-A has changed from 2.03 to 1.98, but this zeolite has a ratio value of more than 1, which is different from the molar ratio of zeolite A in general. For example, zeolite A with a Si/Al molar ratio more than 1 was zeolite ZK-4 [30]. Thus, the used zeolite material is still a group of zeolite A. This study still uses the term zeolite A because the complexity of dimensions, structure and impurities are the same as zeolite A [32].
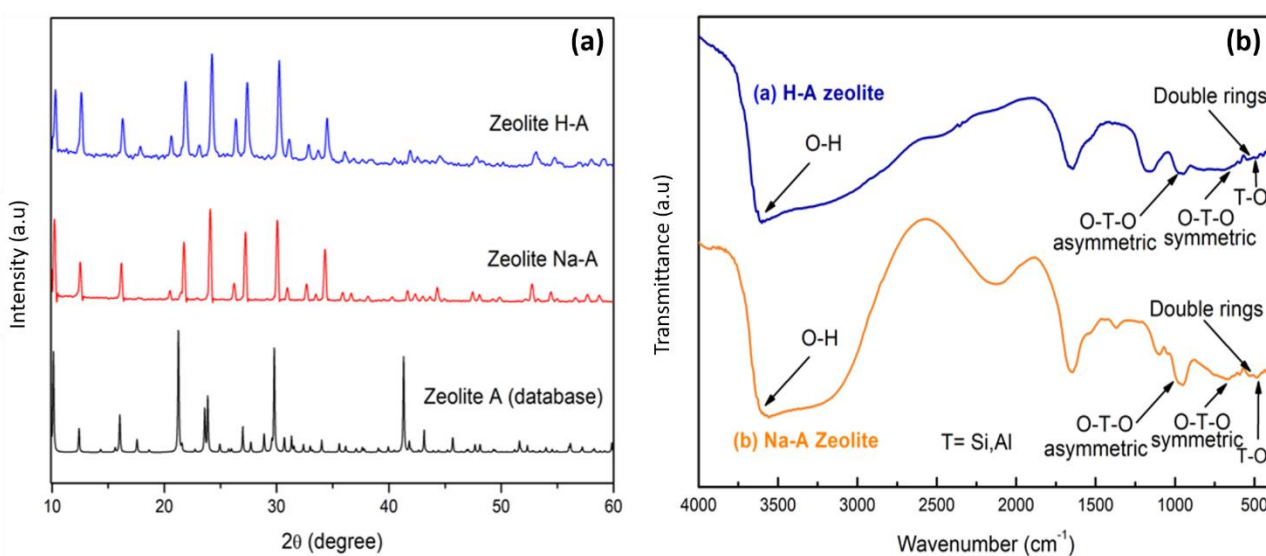

Figure 1. XRD pattern (a) and FTIR (b) of zeolite H-A and zeolite A.

Table 1. XRF results for activation of zeolite A.

Pretreatment	Al	Si	Na	P	K	Ti	Cr	Fe	Ni	Cu	Ba	Yb
Zeolite A (%)	31.8	64.7	5.7	1.3	0.62	0,97	0.11	0.23	0.054	0.14	-	-
Zeolite H-A (%)	32.8	65.0	3.3	-	0.31	0,90	0.096	0.24	0.01	0.11	0.2	0.2

The SEM results are shown in Figure 2. Figure 2a presented a typical cube-shaped micrograph with zeolite LTA morphology [30]. Figure 2b presented a micrograph of the pretreated zeolite that is not different from the initial zeolite. The zeolite has a uniform size even though there is a small

crystal size around it. This shows the zeolite pretreatment from Na-A to H-A does not damage the initial zeolite structure. The average particle sizes of zeolite Na-A and H-A were 516.50 nm and 511.74 nm.
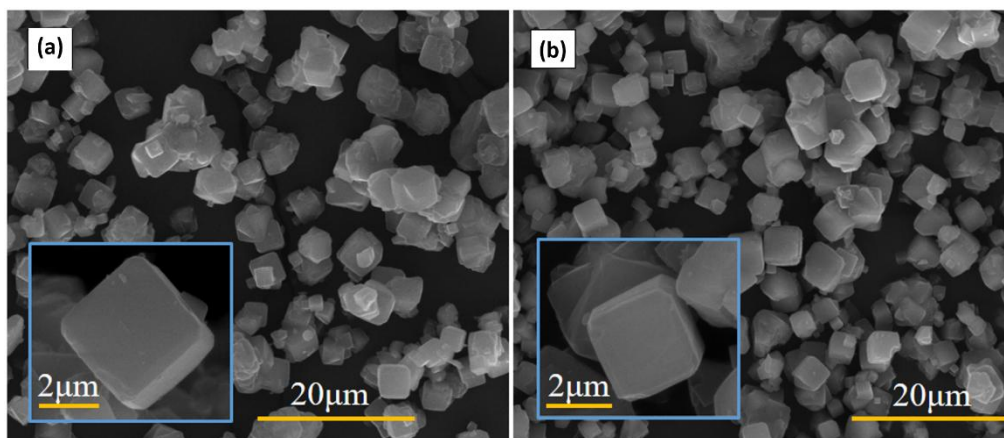

Figure 2. SEM of (a) zeolite Na-A and (b) zeolite H-A.

3.2. Characterization of Fe-TiO₂/zeolite H-A photocatalyst

XRD patterns of TiO_2, Fe-TiO_2, zeolite H-A, TiO_2/zeolite H-A and Fe-TiO_2/zeolite H-A are shown in Figure 3. The used TiO_2 showed sharp peaks at $2\theta = 25.34°$, $37.83°$, $48.07°$, $53.92°$, $55.09°$, $62.72°$, and these peaks indicated an anatase structure, which is in accordance with JCPDS card No. 21-1272 [33,34]. The XRD pattern of Fe-TiO_2 did not show a significant diffractogram difference with pure TiO_2, as well as the characteristic peak of anatase at $2\theta = 25.3274°$. After the impregnation, no diffractogram pattern related to the characteristics of Fe element was observed. This is possible because the amount of the added $Fe(NO_3)_3 \cdot 9H_2O$ powder was too low, so it is difficult to detect in XRD. On the other hand, the size of the Fe^{3+} ion radius (0.69 Å) is almost the same as the Ti^{4+} ion (0.74 Å), so Fe^{3+} ions can easily replace Ti^{4+} ions and combine into the structure of TiO_2 [35]. The XRD results show that there is no significant difference between TiO_2/zeolite H-A and Fe-TiO_2/zeolite H-A. XRD peaks at $2\theta = 25.34°$ (TiO_2/zeolite H-A) and $2\theta = 25.31°$ (Fe-TiO_2/zeolite H-A) indicate the presence of an anatase phase of TiO_2 and a typical zeolite diffractogram pattern, respectively. This shows that the addition of Fe^{3+} impregnation does not change the phase of TiO_2. Further characterization was carried out by looking at the elemental composition using XRF. The results of XRF characterization can be seen in Table 2.
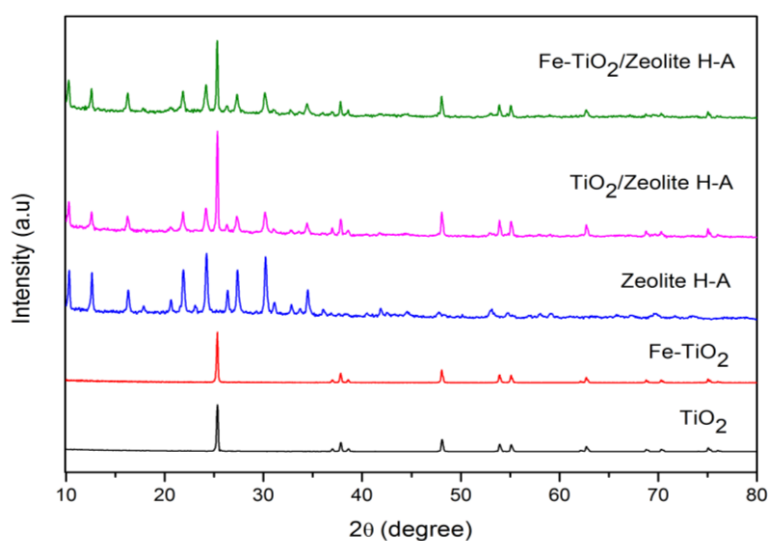
Figure 3. XRD pattern of TiO₂, Fe-TiO₂, zeolite H-A, TiO₂-zeolite H-A and Fe-TiO₂/zeolite H-A.

Table 2. XRF results of TiO₂, Fe-TiO₂, zeolite H-A, TiO₂/zeolite H-A, Fe-TiO₂/zeolite H-A.

Content (%)	TiO₂	Fe-TiO₂	Zeolite H-A	TiO₂/zeolite H-A	Fe-TiO₂/zeolite H-A
Ti	98.74	97.46	0.1	53.8	41.1
Fe	-	1.01	0.24	0.15	0.723
Si	-	-	65.0	26.7	23.2
Al	-	-	32.8	19.5	33.1
P	0.22	0.18	-	-	0.56
Ca	0.11	-	-	-	-
Z	0.22	-	-	-	-
Tm	0.21	-	-	-	-
W	0.24	-	-	-	-
Re	0.05	-	-	-	-
Pt	0.20	0.31	-	-	-
Os	-	0.91	-	-	-
Cu	-	-	0.11	0.10	0.096

Based on Table 2, the composition of the synthesized Fe-TiO₂/zeolite H-A photocatalyst consisted of Ti (TiO₂), Fe, Si and Al (zeolite component) with elemental contents of 41.1%, 0.723%, 23.2% and 33.1%, respectively. This confirmed that the synthesis of Fe-TiO₂/zeolite H-A photocatalyst was successfully carried out. However, from XRF and XRD results, it is not certain whether Fe-TiO₂ and TiO₂ have been evenly dispersed into the external surface of the zeolite.

The FT-IR measurement is carried out with a wavenumber range of 4000–400 cm^{-1}. The FT-IR spectra of TiO₂, Fe-TiO₂, zeolite H-A, TiO₂/zeolite H-A and Fe-TiO₂/zeolite are presented in Figure 4. The absorption band at 1400–400 cm^{-1} was a typical absorption band for zeolite A. In addition, absorption bands appeared at 705.91 cm^{-1} (symmetric) and 1002.16 cm^{-1} (asymmetry) of stretching vibrations of the T-O-T group (T = Si, Al). The absorption at 1644.7 cm^{-1} confirmed the stretching vibration of the O-H group produced from the silanol group (Si-O-H) and was strengthened by the

appearance of the bending vibration of the O-H group of H_2O which was adsorbed on the absorption band 3306–3562 cm^{-1}. The TiO_2 in the zeolite surface was confirmed by the appearance of absorption at 491.85–1049.28 cm^{-1}, which was the vibrational absorption of the Ti-O-Ti group [36]. The impregnation of Fe^{3+} ions into the TiO_2 structure gave rise to new absorption at a wavenumber of 1063 cm^{-1}, which indicated the presence of vibrations from the Fe-O group. Previous studies reported that absorption at 1054–1065 cm^{-1} indicated Fe-O vibrations [37]. Overall, the spectrum can be observed to have a typical absorption of each component and does not overcome a significant spectrum shift in the final structure of the synthesized Fe-TiO_2/zeolite H-A photocatalyst. This indicated that the photocatalyst was reacted without any particular reaction [9].
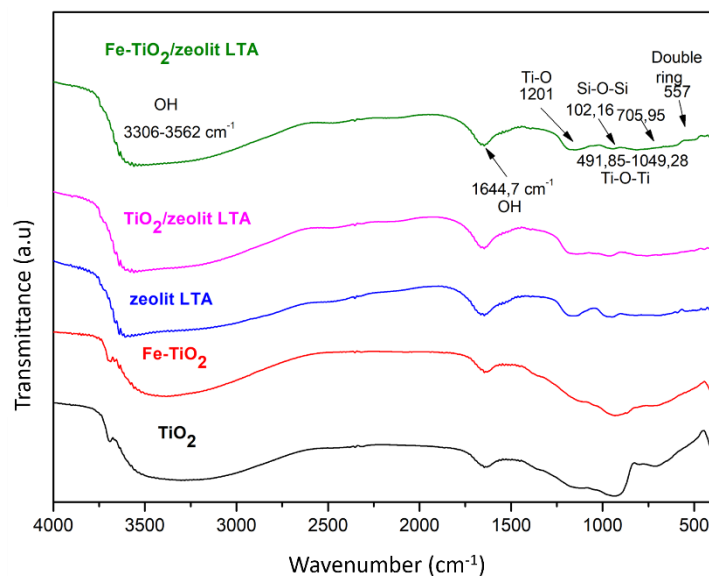

Figure 4. Comparison of the FT-IR Spectra of pure TiO_2, Fe-TiO_2, Zeolite H-A, TiO_2/zeolite H-A and Fe-TiO_2/zeolite H-A.

The SEM results are presented in Figure 5. The surface morphologies of TiO_2 and Fe-TiO_2 have no significant differences in shape and changes. The surface morphologies were spherical, and agglomerate with average particle sizes of 40.96 nm (TiO_2) and 40.56 nm (Fe-TiO_2), respectively. Figure 5c shows the surface morphology of the zeolite H-A with an average particle size of 511.74 nm. Figure 5d shows a change in the surface morphology of the zeolite after TiO_2 addition. It was observed that the TiO_2 agglomerates spread over the surface of the zeolite framework [38,39]. The photocatalyst micrograph of Fe-TiO_2/zeolite H-A in Figure 5e shows that more agglomerates are spread over the surface of the zeolite and cover the surface of the zeolite H-A framework, so the surface becomes rough and uneven after the addition of Fe in TiO_2. This indicates that Fe-TiO_2 has been well distributed on the surface of the zeolite and there is no typical change in morphology of zeolite after the addition of Fe-TiO_2 [5]. The average particle size of the Fe-TiO_2/zeolite H-A photocatalyst was 491.49 nm, and TiO_2/zeolite H-A was 487.29 nm.
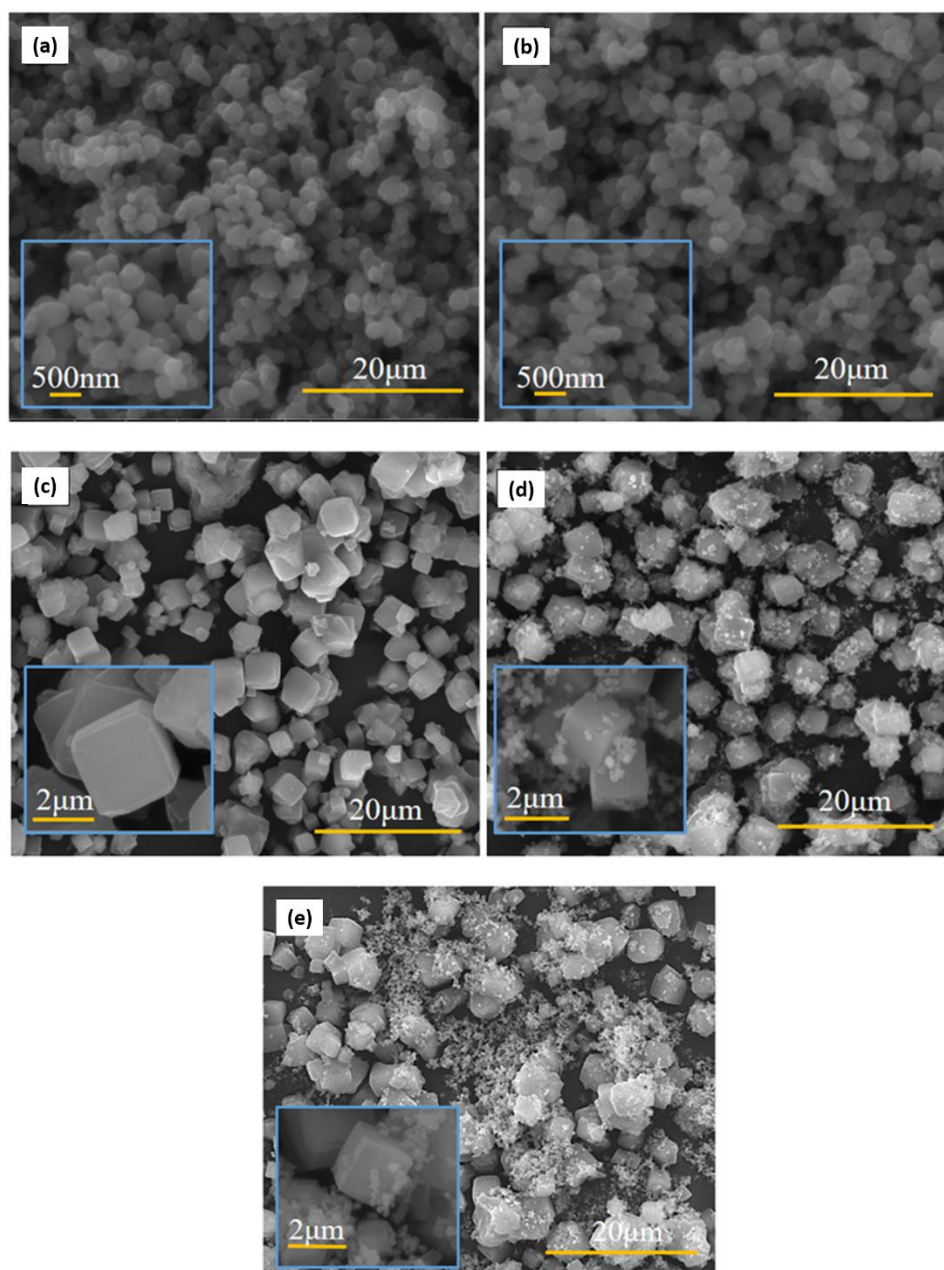
Figure 5. SEM results from (a) TiO_2, (b) Fe-TiO_2, (c) Zeolite H-A, (d) TiO_2/zeolite H-A and (e) Fe-TiO_2/zeolite H-A.

DRS analysis was used to investigate the optical properties of the synthesized photocatalyst. UV-Vis DRS analysis (Figure 6) was carried out at a wavelength of 200–1100 nm, and then the Tauc plot shown in Figure 7 was created. The energy band gaps of Fe-TiO_2, TiO_2/zeolite H-A and Fe-TiO_2/zeolite H-A obtained from the calculation of the Tauc plot (Figure 7a–c) were 3.18 eV, 3.24 eV and 3.16 eV, respectively. These results indicated that the energy band gap of the Fe-TiO_2/zeolite H-A photocatalyst has the smallest value. In addition, there was a decrease in the band gap after TiO_2 was added with Fe^{3+} ion and the zeolite. This indicates that the reducing of the energy band gap has been achieved.
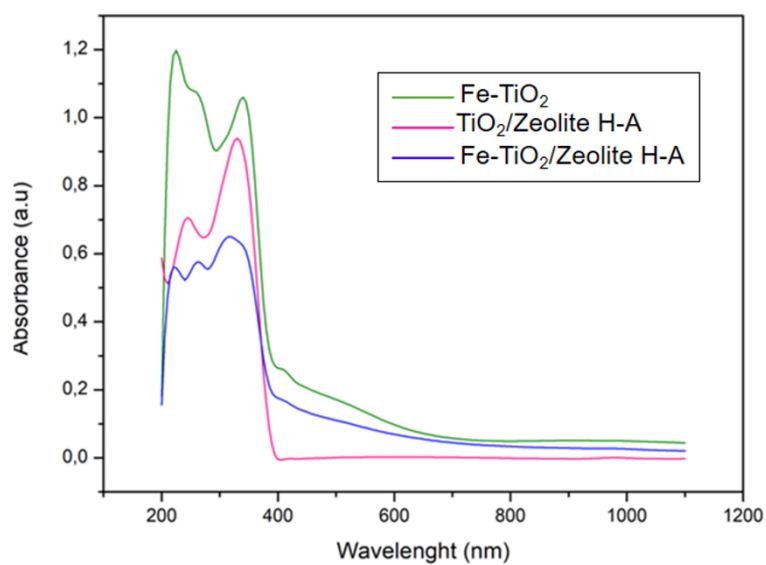
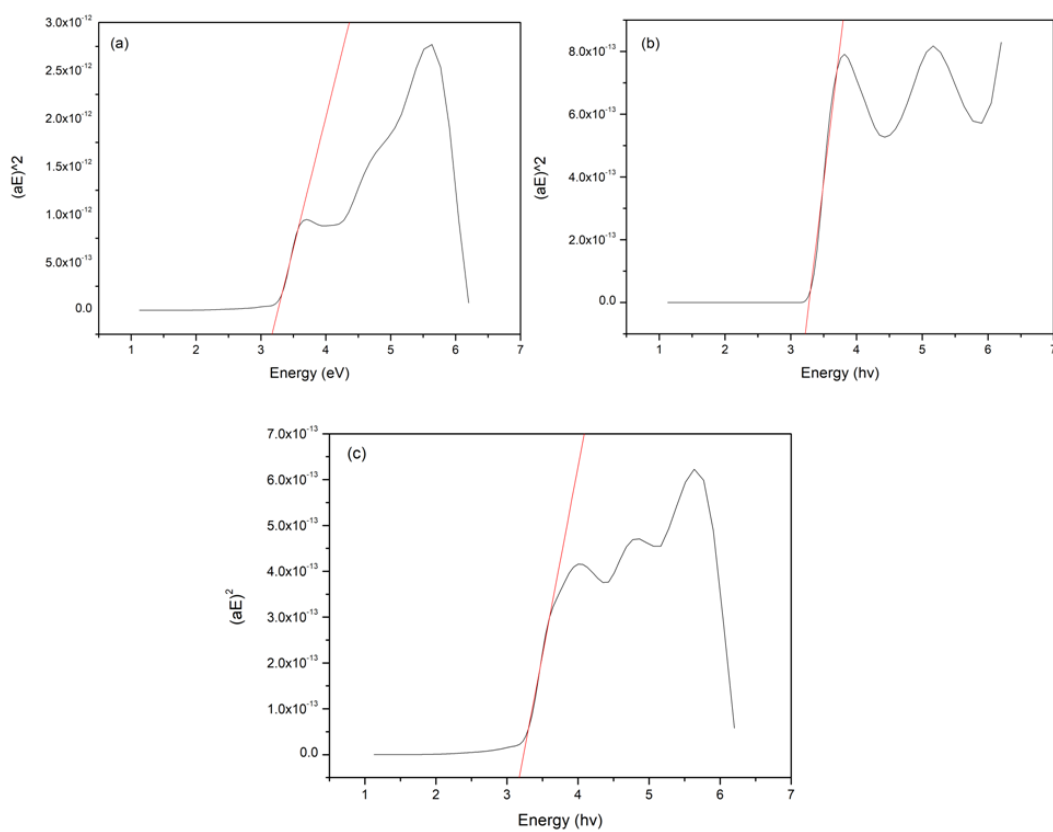**Figure 6.** UV-Vis/DRS spectra of the photocatalyst.

Figure 7. Result of Tauc plots for (a) Fe-TiO$_2$, (b) TiO$_2$/zeolite H-A and (c) Fe-TiO$_2$/zeolite H-A.

3.3. Study of the photocatalytic degradation

Methylene blue degradation with Fe-TiO$_2$/zeolite H-A through a photocatalytic process can be seen in Figure 8.
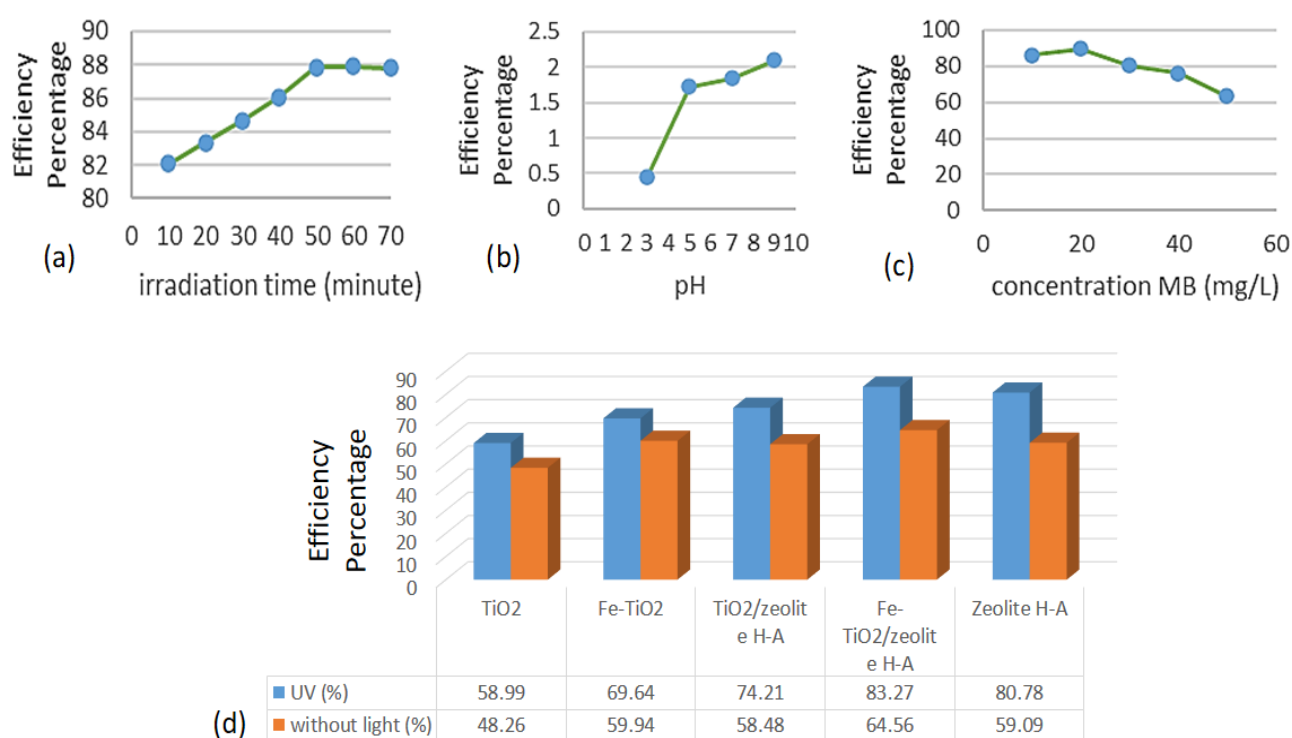
Figure 8. Methylene blue degradation: Efficiency percentage versus Irradiation (a), pH (b), dye concentration (c) and the photocatalyst (d).

Based on Figure 8, the optimum irradiation time of the Fe-TiO$_2$/zeolite H-A photocatalyst to degrade methylene blue was 50 min with a degradation of 87.87%. After it, the decrease of irradiation time occurred due to the Fe-TiO$_2$/zeolite H-A photocatalyst being saturated. Moreover, pH plays a very important role in the formation of hydroxyl radicals (OH•) [40]. The optimum pH was pH 9, because methylene blue is a cationic dye (positive charge), so at alkaline pH it can increase the photocatalytic degradation. At alkaline pH, the surface of TiO$_2$ is negatively charged, which causes an increase in the electrostatic attraction between methylene blue and TiO$_2$ in the photocatalyst. This can be explained by the theory of pH$_{pzc}$ (pH $_{\text{Point of Zero Charge}}$). TiO$_2$ has a pH$_{pzc}$ value of 6.8 when the oxide surface is uncharged. The surface of TiO$_2$ is positively charged when the pH value is less than 6.8 (acidic pH) and negatively charged when pH more than 6.8 (alkaline pH). Finally, efficiency percentage of methylene blue degradation increased with increasing initial methylene blue concentration until it reached a certain limit and then decreased with increasing concentration. Optimum concentration of Methylene Blue was 20 mg/L. If a small amount of UV light reaches the photocatalyst, then the number of electrons will reduce [41]. The presence of zeolite as a support for TiO$_2$ will result in the preservation of nearby dye molecules, thereby increasing the rate of degradation [5]. Another reason is that, with the presence of Fe element and zeolite H-A as a photocatalyst, Fe-TiO$_2$/zeolite H-A has a smaller band gap energy than pure TiO$_2$. The narrower energy band gap means that the distance between the valence band and the conduction band is narrower, so electron excitation is easier, and consequently photocatalytic activity is increasing [42]. So, the degradation performance of the modified TiO$_2$ was higher than the pure TiO$_2$ [43].

4. Conclusions

Fe-TiO$_2$/zeolite H-A photocatalyst was synthesized using the impregnation method. The synthesized photocatalyst was used for the cationic degradation of methylene blue as a model pollutant in wastewater. The successful synthesis of Fe-TiO$_2$/zeolite H-A was proven by XRD, SEM, FT-IR and UV-Vis/DRS. XRD results at 2θ = 25.3 ° showed an anatase phase of the photocatalyst, SEM results showed particle size about 491.49 nm, FT-IR analysis obtained typical bands of zeolite at wavenumbers 490 and 1720 cm^{-1}, and the absorption appeared at 491.85–1049.28 cm^{-1}, which was the vibrational absorption of the Ti-O-Ti group. The addition of Fe^{3+} ions into the TiO$_2$ structure gave rise to new absorption at 1063 cm^{-1}, which indicated the presence of vibrations from the Fe-O group. The band gap width of the synthesized nanocomposite was 3.16 eV, and this value was very close to the band gap of pure TiO$_2$. Furthermore, the photocatalytic efficiency of Fe-TiO$_2$/zeolite H-A against methylene blue was 89.58% with optimum conditions: irradiation time of 50 minutes, pH 9 and concentration of methylene blue about 20 mg/L. The Fe-TiO$_2$/zeolite H-A photocatalyst has been successfully synthesized and can be developed as a promising photocatalyst for the degradation of wastewater dyes.

Acknowledgments

Conflict of interests

The authors stated that there is no conflict of interest for the study.

References

1. Areerob Y, Cho KY, Oh WC (2017) Microwave assisted synthesis of graphene-Bi$_8$La$_{10}$O$_{27}$-Zeolite nanocomposite with efficient photocatalytic activity towards organic dye degradation. *J Photoch Photobio A* 340: 157–169. https://doi.org/10.1016/j.jphotochem.2017.03.018
2. Karuppasamy P, Nisha NRN, Pugazhendhi A, et al. (2021) An investigation of transition metal doped TiO$_2$ photocatalysts for the enhanced photocatalytic decoloration of methylene blue dye under visible light irradiation. *J Environ Chem Eng* 9: 105254. https://doi.org/10.1016/j.jece.2021.105254
3. Qaderi J, Mamat CR, Jalil AA (2021) Preparation and characterization of copper, iron, and nickel doped titanium dioxide photocatalysts for decolorization of methylene blue. *Sains Malays* 50: 135–149. https://doi.org/10.17576/jsm-2021-5001-14
4. Javanbakht V, Ghoreishi SM (2017) Application of response surface methodology for optimization of lead removal from an aqueous solution by a novel superparamagnetic nanocomposite. *Adsorpt Sci Technol* 35: 241–60. https://doi.org/10.1177/0263617416674474

5. Aghajari N, Ghasemi Z, Younesi H, et al. (2019) Synthesis, characterization and photocatalytic application of Ag-doped Fe-ZSM-5@TiO$_2$ nanocomposite for degradation of reactive red 195 (RR 195) in aqueous environment under sunlight irradiation. *J Environ Health Sci* 17: 219–232. https://doi.org/10.1007/s40201-019-00342-5

6. Znad H, Abbas K, Hena S, et al. (2018) Synthesis a novel multilamellar mesoporous TiO$_2$/ZSM-5 for photo-catalytic degradation of methyl orange dye in aqueous media. *J Environ Chem Eng* 6: 218–227. https://doi.org/10.1016/j.jece.2017.11.077

7. Shan AY, Ghazi TIM, Rashid SA (2010) Immobilisation of titanium dioxide onto supporting materials in heterogeneous photocatalysis: A review. *Appl Catal A-Gen* 389: 1–8. https://doi.org/10.1016/j.apcata.2010.08.053

8. Vaez Z, Javanbakht V (2020) Synthesis, characterization and photocatalytic activity of ZSM-5/ZnO nanocomposite modified by Ag nanoparticles for methyl orange degradation. *J Photoch Photobiol A* 388: 112064. https://doi.org/10.1016/j.jphotochem.2019.112064

9. Badvi K, Javanbakht V (2021) Enhanced photocatalytic degradation of dye contaminants with TiO$_2$ immobilized on ZSM-5 zeolite modified with nickel nanoparticles. *J Clean Prod* 280: 124518. https://doi.org/10.1016/j.jclepro.2020.124518

10. Massoudinejad M, Sadani M, Gholami Z, et al. (2019) Optimization and modeling of photocatalytic degradation of Direct Blue 71 from contaminated water by TiO$_2$ nanoparticles: Response surface methodology approach (RSM). *Iran J Catal* 9: 121–132.

11. Ghasemi Z, Younesi H, Zinatizadeh AA (2016) Preparation, characterization and photocatalytic application of TiO$_2$/Fe-ZSM-5 nanocomposite for the treatment of petroleum refinery wastewater: Optimization of process parameters by response surface methodology. *Chemosphere* 159: 552–564. https://doi.org/10.1016/j.chemosphere.2016.06.058

12. Safajou H, Khojasteh H, Salavati-niasari M, et al. (2017) Enhanced photocatalytic degradation of dyes over graphene/Pd/TiO$_2$ nanocomposites: TiO$_2$ nanowires versus TiO$_2$ nanoparticles. *J Colloid Interf Sci* 498: 423–432. https://doi.org/10.1016/j.jcis.2017.03.078

13. Bian H, Zhang Z, Xu X, et al. (2020) Photocatalytic activity of Ag/ZnO/AgO/TiO$_2$ composite. *Physica E* 124: 114236. https://doi.org/10.1016/j.physe.2020.114236

14. Derakhshan-Nejad A, Rangkooy HA, Cheraghi M, et al. (2020) Removal of ethyl benzene vapor pollutant from the air using TiO$_2$ nanoparticles immobilized on the ZSM-5 zeolite under UVradiation in lab scale. *J Environ Health Sci* 18: 201–209. https://doi.org/10.1007/s40201-020-00453-4

15. Pedroza-herrera G, Medina-ram fez IE, Lozano-álvarez JA, et al. (2020) Evaluation of the photocatalytic activity of copper doped TiO$_2$ nanoparticles for the purification and/or disinfection of industrial effluents. *Catal Today* 341: 37–48. https://doi.org/10.1016/j.cattod.2018.09.017

16. Al-Mamun MR, Kader S, Islam MS, et al. (2019) Photocatalytic activity improvement and application of UV-TiO$_2$ photocatalysis in textile wastewater treatment: A review. *J Environ Chem Eng* 7: 103248. https://doi.org/10.1016/j.jece.2019.103248

17. Arifiyana D, Murwani IK (2013) Pengaruh doping Logam Fe pada CaF$_2$ terhadap Struktur Ca$_{1-x}$Fe$_x$F$_2$. *J Sains dan Seni Pomits* 2: 54–56.

18. Khatamian M, Hashemian S, Yavari A, et al. (2012) Preparation of metal ion (Fe^{3+} and Ni^{2+}) doped TiO$_2$ nanoparticles supported on ZSM-5 zeolite and investigation of its photocatalytic activity. *Mater Sci Eng B-Adv* 177: 1623–1627. https://doi.org/10.1016/j.mseb.2012.08.015

19. Khairy M, Zakaria W (2014) Effect of metal-doping of TiO_2 nanoparticles on their photocatalytic activities toward removal of organic dyes. *Egypt J Pet* 23: 419–426. https://doi.org/10.1016/j.ejpe.2014.09.010

20. Hosseini MS, Ebratkhahan M, Shayegan Z, et al. (2020) Investigation of the effective operational parameters of self-cleaning glass surface coating to improve methylene blue removal efficiency; application in solar cells. *Sol Energy* 207: 398–408. https://doi.org/10.1016/j.solener.2020.06.109

21. Noorjahan M, Kumari VD, Subrahmanyam M, et al. (2004) A novel and efficient photocatalyst: TiO_2-HZSM-5 combinate thin film. *Appl Catal B-Environ* 47: 209–213. https://doi.org/10.1016/j.apcatb.2003.08.004

22. Mahalakshmi M, Priya SV, Arabindoo B, et al. (2009) Photocatalytic degradation of aqueous propoxur solution using TiO_2 and Hβ zeolite-supported TiO_2. *J Hazard Mater* 161: 336–343. https://doi.org/10.1016/j.jhazmat.2008.03.098

23. Loiola AR, Andrade JCRA, Sasaki JM, et al. (2012) Structural analysis of zeolite NaA synthesized by a cost-effective hydrothermal method using kaolin and its use as water softener. J *Colloid Interf Sci* 367: 34–39. https://doi.org/10.1016/j.jcis.2010.11.026

24. Wuntu AD, Kamu VS, Kumaunang M (2019) Crystallization temperature of NaA zeolite prepared from gel and aluminum hydroxide. *Chem Prog* 4: 1–4.

25. Afrozi AS, Salam R, R A, et al. (2016) Pengolahan limbah methylen blue secara fotokatalisis TiO_2 dengan penambahan Fe dan zeolit. *Prosiding Seminar Nasional Teknologi Pengelolaan Limbah*, 29–36. Available from: http://repo-nkm.batan.go.id/7417/.

26. Pratama NA, Artsanti P (2019) Effect of aeration treatment on methylene blue removal using TiO_2-zeolite. *Proceeding International Conference on Science and Engineering* 2: 219–224. https://doi.org/10.14421/icse.v2.89

27. Estiaty LM (2015) Synthesis and characterization of zeolite-TiO_2 from modified natural zeolite. *Teknol Miner dan Batubara* 11: 181–190.

28. Erwanto E, Yulinda Y, Nabela Q (2020) Pengaruh Penambahan Ion Nitrat (NO_3^-) terhadap Kinetika Fotodegradasi Zat Warna Metilen Biru Menggunakan Zeolit-TiO_2. *J Inovasi Teknik Kimia* 5: 59–67. Available from: http://dx.doi.org/10.31942/inteka.v5i2.3812.

29. Septian DD, Sugiarti S (2019) Modifikasi Zeolit Alam Ende dengan Garam Logam serta Potensinya Sebagai Katalis Transformasi Glukosa Menjadi 5-Hidroksimetilfurfural (HMF). *ALCHEMY J Penelit Kim* 15: 203–218. https://doi.org/10.20961/alchemy.15.2.28180.203-218

30. Rigo RT, Prigol C, Antunes Â, et al. (2013) Synthesis of ZK4 zeolite: An LTA-structured zeolite with a Si/Al ratio greater than 1. *Mater Lett* 102: 87–90. https://doi.org/10.1016/j.matlet.2013.03.120

31. Ginting SB, Sari DP, Iryani DA, et al. (2019) Sintesis ZeolitT Lynde Type-A (LTA) Dari Zeolit Alam Lampung (ZAL) Menggunakan Metode Step Change Temperature Of Hydrotermal Dengan Variasi SiO_2/Al_2O_3 Diaplikasikan Untuk Dehidrasi Etanol. *J Chem Process Eng* 4: 32–44. https://doi.org/10.33536/jcpe.v4i1.324

32. Asrori MR, Santoso A, Sumari S (2022) Initial defect product on immiscible mixture of palm oil: Ethanol by amphiphilic chitosan/Zeolite LTA as optimization of microemulsion fuel. *Ind Crops Prod* 180: 114727. https://doi.org/10.1016/j.indcrop.2022.114727

33. Treacy MMJ, Higgins JB (2007) *Collection of Simulated XRD Powder Patterns for Zeolites*, 5 Eds., Elsevier.

34. Sescu AM, Favier L, Lutic D, et al. (2021) TiO$_2$ doped with noble metals as an efficient solution for the photodegradation of hazardous organic water pollutants at ambient conditions. Water (Switzerland) 13: 1–18. https://doi.org/10.3390/w13010019

35. Sood S, Umar A, Mehta SK, et al. (2015) Highly effective Fe-doped TiO$_2$ nanoparticles photocatalysts for visible-light driven photocatalytic degradation of toxic organic compounds. *J Colloid Interf Sci* 450: 213–223. https://doi.org/10.1016/j.jcis.2015.03.018

36. Cacciato G, Zimbone M, Ruffino F, et al. (2016) TiO$_2$ nanostructures and nanocomposites for sustainable photocatalytic water purification, In: Larramendy ML, Soloneski S, *Green Nanotechnology-Overview and Further Prospects*, Croatia: Janeza Trdine. https://doi.org/10.5772/62620

37. Pratiwi E, Harlia H, Aritonang AB (2020) Sintesis TiO$_2$ terdoping Fe^{3+} untuk Degradasi Rhodamin B Secara Fotokatalisis dengan Bantuan Sinar Tampak. *Positron* 10: 57–63. https://doi.org/10.26418/positron.v10i1.37739

38. Al-Harbi LM, Kosa SA, Abd El Maksod IH, et al. (2015) The photocatalytic activity of TiO$_2$-zeolite composite for degradation of dye using synthetic UV and Jeddah sunlight. *J Nanomater* 16: 46. https://doi.org/10.1155/2015/565849

39. Li H, Zhang W, Liu Y (2020) HZSM-5 zeolite supported boron-doped TiO$_2$ for photocatalytic degradation of ofloxacin. *J Mater Res Technol* 9: 2557–2567. https://doi.org/10.1016/j.jmrt.2019.12.086

40. Sahel K, Perol N, Chermette H, et al. (2007) Photocatalytic decolorization of Remazol Black 5 (RB5) and Procion Red MX-5B-Isotherm of adsorption, kinetic of decolorization and mineralization. *Appl Catal B-Environ* 77: 100–109. https://doi.org/10.1016/j.apcatb.2007.06.016

41. Khan I, Saeed K, Zekker I, et al. (2022) Review on methylene blue: Its properties, uses, toxicity and photodegradation. *Water* 14: 242. https://doi.org/10.3390/w14020242

42. Sutanto H, Wibowo S (2015) Semikonduktor Fotokatalis Seng Oksida dan Titania: Sintesis, Deposisi dan Aplikasi. Available from: http://eprints.undip.ac.id/49049/.

43. Asiltürk M, Sayılkan F, Arpaç E (2009) Effect of Fe^{3+} ion doping to TiO$_2$ on the photocatalytic degradation of Malachite Green dye under UV and vis-irradiation. *J Photoch Photobiol A* 203: 64–71. https://doi.org/10.1016/j.jphotochem.2008.12.021